

Received December 3, 2020, accepted December 14, 2020, date of publication December 23, 2020, date of current version January 5, 2021.

Digital Object Identifier 10.1109/ACCESS.2020.3046853

Regenerative Braking Control Method Based on Predictive Optimization for Four-Wheel Drive Pure Electric Vehicle

JUNJIANG ZHANG¹, YANG YANG^{1,2}, (Member, IEEE), DATONG QIN^{1,2}, (Member, IEEE),
CHUNYUN FU^{1,2}, AND ZHIPENG CONG¹

¹School of Automotive Engineering, Chongqing University, Chongqing 400044, China

²State Key Laboratory of Mechanical Transmissions, Chongqing University, Chongqing 400044, China

Corresponding author: Yang Yang (yangyang@cqu.edu.cn)

This work was supported in part by the National Key Research and Development Program of China under Grant 2018YFB0106100, and in part by the Natural Science Foundation of China under Grant 51575063.


ABSTRACT Regenerative braking is the key to achieve efficient use of energy and extend the driving range in pure electric vehicles. This study proposes a new predictive control method integrating adaptive cubic exponential prediction and dynamic programming to address the problem of efficient energy recovery during the regular braking process of four-wheel pure electric vehicles. The method considers the dynamic characteristics of an electro-hydraulic combined braking system. The adaptive cubic exponential prediction is adopted to predict the vehicle velocity and braking intensity. The dynamic programming is employed to optimize the motor braking torques and wheel cylinder pressures under the condition of braking regulations, road constraints, and vehicle constraints. To verify the effectiveness of the new predictive control method, the ideal and multi-stage braking force distribution methods are employed for comparison. The results confirm that, under gradual braking conditions, the energy recovery efficiency achieved via the proposed method is improved by 1.55% and 6.40% considering the ideal and multi-stage braking force distribution methods, respectively.

INDEX TERMS Pure electric vehicle, energy recovery, dynamic characteristics, adaptive cubic exponential, dynamic programming.

I. INTRODUCTION

As the development of zero-emission pure electric vehicles is beneficial to the global environment [1]–[3], they are being increasingly developed and deployed worldwide [4].

Some researchers have conducted in-depth studies on electric vehicles, including handling stability control [5], yaw stability control [6], and inertial estimation [7]. However, the short driving range of these vehicles hinders their promotion and application. Research indicates that 50% of the energy of pure electric vehicles is wasted in the form of heat by a conventional braking system during deceleration in urban conditions [8]. Therefore, studies on the regenerative braking energy recovery of pure electric vehicles are necessary [9]–[11].

The associate editor coordinating the review of this manuscript and approving it for publication was Wei Xu .

The existing studies aiming to improve the energy recovery of regenerative braking mainly focus on two groups: system design and control [12]–[15]. Regarding system design, supercapacitors [16] or flywheels [17] are added in some studies to increase energy recovery, which can improve energy conversion efficiency. Regarding system control, in [18], model predictive control was applied to distribute braking energy for battery and supercapacitors, and a satisfactory control effect was obtained. However, these approaches increase both the complexity of the system and the cost of the entire vehicle owing to the addition of supercapacitors or flywheels. Thus, the recovery of kinetic energy by the motor becomes the best choice in all types of vehicles, as a trade-off between performance and cost [19].

The energy recovery is closely related to the braking control method when only the motor recovers the braking kinetic energy. An adequate braking control method can improve the energy recovery efficiency, whereas an inadequate method

may cause the energy recovery effect to deteriorate, and even threaten the braking safety of the vehicle. In recent years, an increasing number of studies has focused on the energy recovery by motor braking. The methods can be further divided into two aspects: rule- and optimization-based control [20]–[23]. Regarding rule-based control, early research mainly considered the regulations of the Economic Commission for Europe (ECE) and ideal braking force distribution [24]. Although this can improve the energy recovery efficiency, it does not consider the driver’s intention recognition. To address driver’s intention recognition, fuzzy logic [25] was adopted and a better energy recovery effect was obtained. To approximate to the actual control situation, system dynamics and driver intention recognition [26], [27] were considered, but only in terms of system modeling and not in terms of method formulation. The above methods are all rule-based, and the energy recovery effect can be further improved through optimization. Fuzzy logic optimized by genetic algorithm [28] was adopted to obtain electro-hydraulic braking force distribution rules. Although this method did not consider the driver’s intention recognition, other studies considered this aspect [29] [30], obtaining an improvement in energy recovery efficiency. However, the dynamic characteristics of the system were neglected, as well as the future state information of the vehicle.

With the development of vehicle electrification and intelligence, energy recovery is an important research focus, whether it is a manually driven vehicle or an intelligent vehicle [31]. This study mainly focuses on the energy recovery of manually driven vehicles. It is well recognized that the dynamic characteristics of the electro-hydraulic combined braking system have an important influence on the control of the vehicle. However, regarding the formulation of regenerative braking methods, the dynamic characteristics of the braking system are rarely considered in existing studies. Neglecting these characteristics may worsen the recovery efficiency. In addition, the future of vehicle state information such as vehicle velocity and braking intensity has also important influence for vehicle energy recovery. If the state of the vehicle is known in advance, it may help to improve the energy recovery. To solve the mentioned issues, a predictive control method (PCM) that centers on the future of vehicle state information and dynamic characteristics of the electro-hydraulic combined braking system is proposed for four-wheel pure electric vehicles to improve energy recovery efficiency. Three vital advantages of the PCM are presented in the study:

- An adaptive cubic exponential prediction is integrated into PCM to solve the problem of obtaining future vehicle state information, such as vehicle velocity and braking intensity;
- A dynamic programming is integrated into PCM to consider dynamic characteristics of the electro-hydraulic combined braking system and obtain the front and rear motor braking torques, and front and rear wheel cylinder pressures;

- A predictive optimization framework of PCM that includes adaptive cubic exponential prediction and dynamic programming is presented for the first time.

The remainder of this paper is organized as follows. Section 2 illustrates the system structure and model of the vehicle, and Section 3 describes the vehicle PCM. The verification and discussion are presented in Section 4, and conclusions are presented in Section 5.

II. SYSTEM STRUCTURE AND MODEL

A. VEHICLE SYSTEM STRUCTURE

The power system of the four-wheel pure electric vehicle is a centralized arrangement of front and rear axle dual motors. The vehicle system, which includes the battery, front and rear motors, main reducers I and II, wheel cylinders, and braking unit are displayed in Figure 1. The battery and the motors are electrically connected. The motors, main reducers, and wheels are mechanically connected, and the wheel cylinders and the braking unit are connected by pipelines.

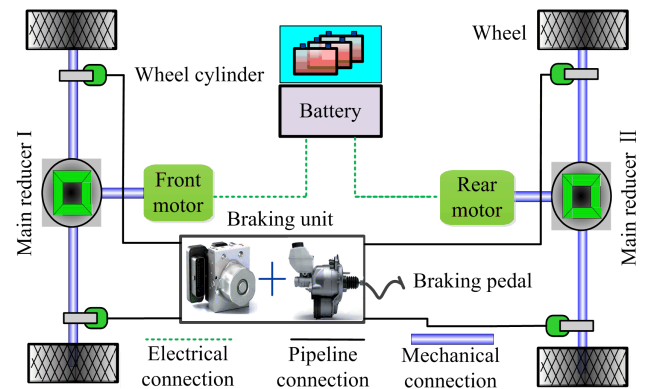


FIGURE 1. Schematic diagram of the vehicle system structure.

B. VEHICLE MODEL

Because only a longitudinal braking analysis is performed in this study, the vehicle model is simplified to a left-right symmetrical model (i.e., the left and right wheel parameters are explained using a single wheel as an example). The established vehicle models include the vehicle dynamics model, efficiency and dynamic models of the motors, internal resistance model of the battery, transmission system, tire, and wheel cylinder models.

1) VEHICLE DYNAMICS MODEL

The vehicle driving equation is important for simulating vehicle driving. According to Newton’s second law, the driving equation during vehicle braking is established as

$$F_b + F_f + F_w + F_i = \delta ma \tag{1}$$

where F_b , F_f , F_w , and F_i denote the vehicle braking force, rolling, wind, and ramp resistances, respectively. δ denotes the vehicle rotation mass conversion factor. m denotes the vehicle curb mass and a denotes the vehicle acceleration.

The vehicle braking intensity is a key parameter of the vehicle and is represented by

$$z = -a/g \tag{2}$$

where z denotes the braking intensity of the vehicle and g denotes the acceleration of gravity.

The load on the front and rear axles for a vehicle changes with modifications in the braking intensity, which is closely related to the generation of tire force. The corresponding mathematical model is as follows:

$$\begin{cases} F_{z1} = mg(b + zh_g)/L \\ F_{z2} = mg(c - zh_g)/L \end{cases} \tag{3}$$

where F_{z1} and F_{z2} denote the front and rear axle loads, respectively. c and b denote the distance from the center of gravity to the front and rear axles, respectively. h_g denotes the height of gravity center and L denotes the wheelbase.

2) MOTOR MODEL

The motor is an essential component for the energy recovery of a four-wheel pure electric vehicle. In this study, the motor model is divided into motor efficiency and dynamic models. The front and rear motors efficiency models are displayed in Figures 2(a) and (b), respectively.

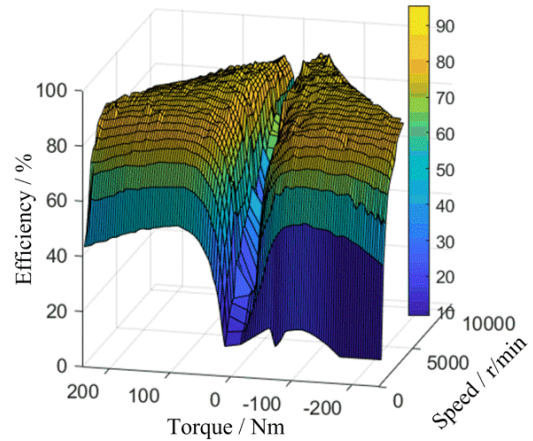
The transfer function and state space methods are commonly used for the modeling of motor dynamic characteristics. The transfer function initial state value is zero; it is difficult to realize the dynamic simulation of a nonzero initial state motor. The torque in the actual control process of the motor is primarily from one torque (nonzero) to another torque (nonzero). In addition, the state-space method can easily set the initial state value. Therefore, this study adopts the state space method to establish the dynamic models of the motors.

$$\begin{cases} \begin{bmatrix} \dot{x}_{1i} \\ \dot{x}_{2i} \end{bmatrix} = \begin{bmatrix} 0 & 1 \\ -a_{2i} & -a_{1i} \end{bmatrix} \begin{bmatrix} x_{1i} \\ x_{2i} \end{bmatrix} + \begin{bmatrix} 0 \\ 1 \end{bmatrix} u_i \\ y_i = \begin{bmatrix} b_{2i} & b_{1i} \end{bmatrix} \begin{bmatrix} x_{1i} \\ x_{2i} \end{bmatrix}, \quad i = 1, 2 \end{cases} \tag{4}$$

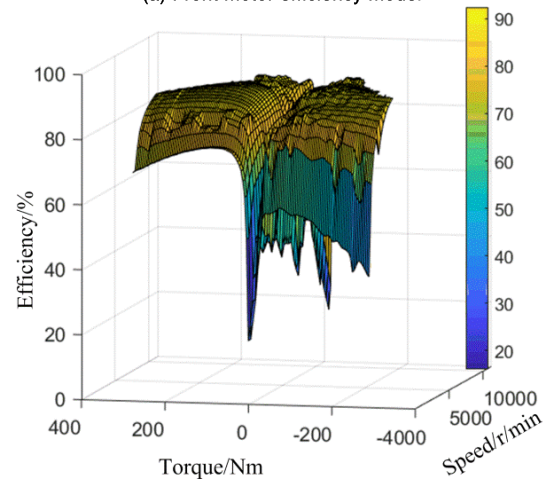
where x_{11} , x_{21} , and x_{12} , x_{22} denote the states of the front and rear motors, respectively. \dot{x}_{11} , \dot{x}_{21} and \dot{x}_{12} , \dot{x}_{22} denote the differentials of the states for the front and rear motors, respectively. u_1 and u_2 denote the input and y_1 and y_2 denote the outputs of the front and rear motors, respectively. a_{11} , a_{21} , b_{11} , b_{21} , a_{12} , a_{22} , b_{12} , b_{22} are constants and reflect the dynamic characteristics of the front and rear motors. Note that these parameters can be obtained through the transfer function. x_{1i} and y_i represent motor output torques.

The power delivered by the motor to the battery in the process of braking is

$$\begin{cases} P_b = P_{b1} + P_{b2} \\ P_{b1} = T_{p1}n_{p1}\eta_{m1}/9550 \\ P_{b2} = T_{p2}n_{p2}\eta_{m2}/9550 \end{cases} \tag{5}$$



(a) Front motor efficiency model



(b) Rear motor efficiency model

FIGURE 2. Motor efficiency models.

where P_b denotes the power transferred from the motor to the battery during braking. P_{b1} and P_{b2} denote the power, T_{p1} and T_{p2} denote the actual braking torque, n_{p1} and n_{p2} denote the speed, and η_{m1} and η_{m2} denote the braking efficiency of the front and rear motors, respectively.

3) TRANSMISSION SYSTEM MODEL

The transmission system of the vehicle is important for vehicle torque transmission. The relationship between the torque and rotation speed of the motor and wheel ends is

$$\begin{cases} T_{pj} = 2\eta_j T_{mdj}/i_j \\ n_{pj} = w_j i_j / (2\pi), \quad j = 1, 2 \end{cases} \tag{6}$$

where η_1 and η_2 denote the transmission system efficiency of the front and rear axles, respectively. i_1 and i_2 denote the transmission ratio of main reducers I and II, respectively. w_1 and w_2 denote the angular speeds of the front and rear wheels, respectively. T_{md1} and T_{md2} denote the braking torque generated by the front motor at the front wheel end and the rear motor at the rear wheel end, respectively.

4) BATTERY MODEL

The battery model adopts the common internal resistance model, as indicated in Figure 3. In this model, the battery is simplified into a system composed of a voltage source and internal resistance. According to Kirchoff's voltage law,

$$E = U + Ir \quad (7)$$

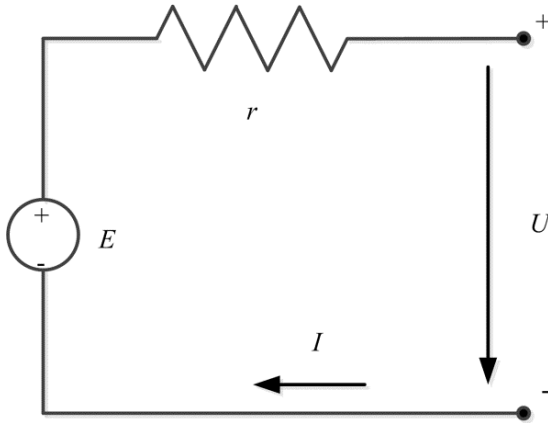


FIGURE 3. Battery internal resistance model.

where E is the battery open circuit voltage, U is the charging voltage, I is the charging current, and r is the battery charging internal resistance

The amount of battery energy recovery is an evaluation index to measure the effect of braking control. It is

$$\begin{cases} |P_b| = |EI| + I^2r \\ Q = - \int |EI|dt \end{cases} \quad (8)$$

where Q denotes the energy recovery of the battery.

5) WHEEL CYLINDER MODEL

The wheel cylinder is directly related to the generation of mechanical braking force. The relationship between the front and rear wheel hydraulic braking torques and wheel cylinder pressure can be obtained using

$$\begin{cases} T_{phf} = p_{pw1} \pi D_f^2 R_f K_f / 4 \\ T_{phr} = p_{pw2} \pi D_r^2 R_r K_r / 4 \end{cases} \quad (9)$$

where T_{phf} and T_{phr} denote the actual hydraulic braking torques of the front and rear wheels, respectively, p_{pw1} and p_{pw2} denote the actual pressures of the front and rear wheel cylinders, respectively, K_f and K_r denote the braking factors of the front and rear axle brakes, respectively, D_f and D_r denote the wheel cylinder diameters of the front and rear wheels, respectively. R_f and R_r denote the effective radius of the front and rear wheel brake discs, respectively.

To more accurately reflect the dynamic characteristics of the hydraulic braking system, the wheel cylinder model is regarded as a first-order inertial link [32], and the dynamic

characteristics can be described using the state space method as

$$\begin{cases} \dot{x}_{ki} = a_{ki}x_{ki} + u_{ki} \\ y_{ki} = b_{ki}x_{ki}, \quad i = 1, 2 \end{cases} \quad (10)$$

where x_{k1} and x_{k2} denote the states, \dot{x}_{k1} and \dot{x}_{k2} denote the differential states, u_{k1} and u_{k2} denote the inputs, and y_{k1} and y_{k2} denote the outputs of the front and rear wheel cylinders, respectively. a_{k1} , b_{k1} , a_{k2} , and b_{k2} are constants related to the dynamic characteristics of each wheel cylinder. Note that these parameters can be obtained through the transfer function and that x_{ki} and y_{ki} represent wheel cylinder braking torques.

6) TIRE MODEL

The tire model in this study includes the wheel dynamics model and magic model.

In the process of vehicle braking, the wheel dynamics model is described by

$$jw_i \dot{w}_i = T_{di} - 0.5u_{xi}Fz_iR_t - 0.5Fz_{ij}fR_t, \quad i = 1, 2 \quad (11)$$

where jw_1 and jw_2 denote the inertia, T_{d1} and T_{d2} denote the braking torque, and u_{x1} and u_{x2} denote the adhesion coefficients of the front and rear wheels, respectively. R_t denotes the wheel radius. The four wheels of the vehicle have the same radius. \dot{w}_1 and \dot{w}_2 denote the angular acceleration of the front and rear wheels, respectively. f denotes the rolling resistance coefficient. i is equal to "1" or "2", representing the front or rear wheel, respectively.

As the magic tire model is a semi-empirical model that can reflect the interaction with the road surface, it is suitable for the dynamic simulation panel of the vehicle [33] and was adopted in this study. Using a single tire as an example, its form is

$$Y(x) = D \sin(C \arctan(Bs - E(Bs - \arctan(Bs)))) \quad (12)$$

where $Y(x)$ denotes the output variable: longitudinal force, and s denotes the slip ratio. B , C , D , and E refer to the stiffness, shape, peak, and curvature factors, respectively.

The slip rate is an important parameter of the tire model; its expression is

$$s_i = (v_x - w_i R_t) / v_x, \quad i = 1, 2 \quad (13)$$

where s_1 and s_2 denote the front and rear wheel slip rates, respectively, and v_x denotes the vehicle velocity.

The motor and hydraulic braking torques are coupled at the wheel. The coupling model is

$$\begin{cases} T_{d1} = T_{phf} + T_{md1} \\ T_{d2} = T_{phr} + T_{md2} \end{cases} \quad (14)$$

The schematic diagram of the vehicle simulation model is displayed in Figure 4. The simulation model includes six parts: the wheel cylinder, motor, transmission system, battery, vehicle dynamics, and tire models. The red dotted enclosure represents the predictive vehicle model (the first four parts).

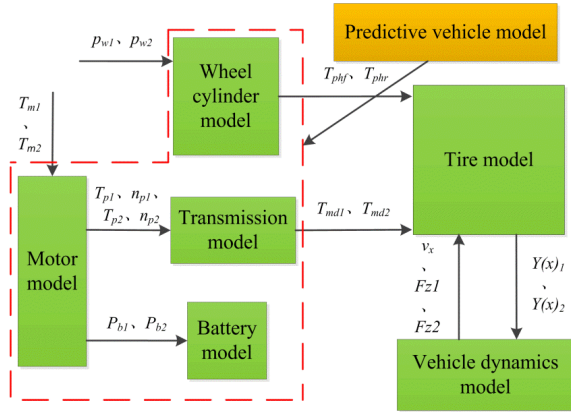


FIGURE 4. Schematic diagram of the vehicle simulation model.

T_{m1} and T_{m2} are the required torques of the front and rear motors, respectively. p_{w1} and p_{w2} are the wheel required cylinder pressures of the front and rear wheels, respectively. $Y(x)_1$ and $Y(x)_2$ are the longitudinal forces generated by the front and rear wheels, respectively. The motor model and wheel cylinder model accept commands ($p_{w1}, p_{w2}, T_{m1}, T_{m2}$), generate braking torques (T_{p1}, T_{p2}) and wheel cylinder pressures (T_{phf}, T_{phr}), and transfer the relevant parameters to the transmission system model ($T_{p1}, n_{p1}, T_{p2}, n_{p2}$), battery model (P_{b1}, P_{b2}), and tire model ($T_{phf}, T_{phr}, T_{md1}, T_{md2}$). The tire model also accepts the parameters (v_x, F_{z1}, F_{z2}) from the vehicle dynamics model and transmits the longitudinal force ($Y(x)_1, Y(x)_2$) to the vehicle dynamics model.

III. PCM DESIGN

Performing data prediction based on the historical data of a vehicle to provide data support for its operation is essential to improve the efficient energy recovery during the braking process of the vehicle. In this study, the adaptive cubic exponential prediction is used to predict the key parameters of the vehicle operation. Based on the dynamic programming, the braking torques and wheel cylinder pressures are optimized under the constraints of ECE braking regulations, vehicle constraints, and motor maximum braking torque to achieve efficient energy recovery. As the adaptive cubic exponential prediction has a better prediction effect on gradual data, the prediction of sudden change data is not ideal. Therefore, this study is suitable for gradual braking intensity conditions. Note that the PCM in this study is employed when the battery state of charge (SOC) does not exceed the specified upper limit.

A. ADAPTIVE CUBIC EXPONENTIAL PREDICTION

The adaptive cubic exponential prediction optimizes the smoothing coefficient based on the cubic exponential smoothing method, obtains the prediction data model with the smallest error, and predicts the future data [34], which has an acceptable prediction effect on time-varying and nonlinear data. The ability of the cubic exponential smoothing method

to adapt to time-varying data is not sufficient. However, the adaptive cubic exponential prediction method overcomes this shortcoming, thus, it was selected. The model of the cubic exponential smoothing is

$$\begin{cases} S_{k,t}^{(1)} = \lambda_k X_{k,t} + (1 - \lambda_k) S_{k,t-1}^{(1)} \\ S_{k,t}^{(2)} = \lambda_k S_{k,t}^{(1)} + (1 - \lambda_k) S_{k,t-1}^{(2)} \\ S_{k,t}^{(3)} = \lambda_k S_{k,t}^{(2)} + (1 - \lambda_k) S_{k,t-1}^{(3)} \end{cases} \quad (15)$$

where $t = 2, 3, 4, \dots$ $S_{k,t}^{(1)}, S_{k,t}^{(2)}$, and $S_{k,t}^{(3)}$ are the first, second, and third exponential smoothing values of the k -th prediction t period data, respectively. $X_{k,t}$ is the k -th prediction t period of the actual data. λ_k is the k -th prediction smoothing coefficient ($0 < \lambda_k < 1$).

To forecast future data, let T be the number of periods predicted forward from time t , and let $a_{k,t}, b_{k,t}$, and $c_{k,t}$ be the prediction coefficients of the k -th prediction

$$\begin{cases} a_{k,t} = 3S_{k,t}^{(1)} - 3S_{k,t}^{(2)} + S_{k,t}^{(3)} \\ b_{k,t} = \lambda((6 - 5\lambda)S_{k,t}^{(1)} - (10 - 8\lambda)S_{k,t}^{(2)} \\ + (4 - 3\lambda)S_{k,t}^{(3)}) / (2(1 - \lambda)^2) \\ c_{k,t} = \lambda^2(S_{k,t}^{(1)} - 2S_{k,t}^{(2)} + S_{k,t}^{(3)}) / (1 - \lambda)^2 \end{cases} \quad (16)$$

The $t + T$ period predicted value of the k -th is

$$Y_{k,t+T} = a_{k,t} + b_{k,t}T + c_{k,t}T^2 \quad (17)$$

where T is the prediction step, that is, the interval between the target prediction period and current period. $T = 1, 2, 3, \dots$ $Y_{k,t+T}$ is the $t + T$ period predicted value of the k -th prediction.

The prediction accuracy is the basis for evaluating the quality of the prediction. This study adopts the sum of squared errors as the basis for evaluation.

$$ff = \min \sum_{i=4}^N (Y_{k,i} - X_{k,i})^2 \quad (18)$$

where ff represents the sum of the squared errors. $Y_{k,i}$ represents the i -th data prediction value of the k -th prediction. $X_{k,i}$ represents the i -th data actual value of the k -th prediction. N is the number of data samples.

The adaptive cubic exponential prediction refers to the optimization of the smoothing coefficients using the carpet traversal search algorithm to obtain dynamic smoothing coefficients

$$\varepsilon_{k,t} = \hat{\lambda}_k / (1 - (1 - \hat{\lambda}_k)^t) \quad (19)$$

where $\varepsilon_{k,t}$ is a function of time t , which represents the dynamic smoothing coefficient at the k -th prediction. $\hat{\lambda}_k$ is the smoothing coefficient after the k -th prediction optimization.

The prediction flow chart of the adaptive cubic exponential prediction is displayed in Figure 5. This prediction first collects the historical data (braking intensity z_k and vehicle velocity v_{xk}) derived from the vehicle simulation model. The carpet traversal search method is used to optimize the smoothing coefficient of the cubic exponential smoothing with the

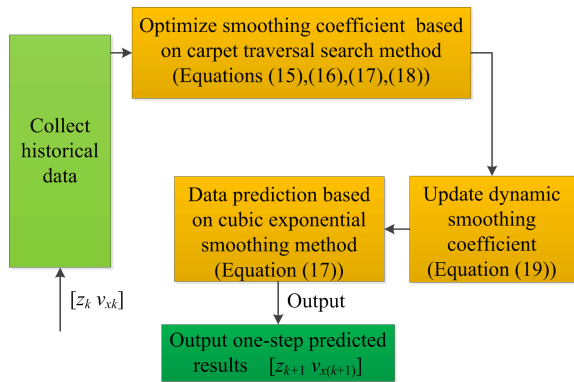


FIGURE 5. Prediction flow chart of adaptive cubic exponential prediction.

smallest square error as the goal (refer to [34] for details). The dynamic smoothing coefficient is updated according to Equation (19). Subsequently, the one-step prediction data (braking intensity z_{k+1} and vehicle velocity $v_{x(k+1)}$) are output, followed by data collection for the next data prediction. For adaptive cubic exponential prediction, one-step prediction results are the most accurate [34], thus they are adopted. In this study, the data predicted by the adaptive cubic exponential prediction and current data are combined into vectors ($[z_k v_{xk}; z_{k+1} v_{x(k+1)}]$) to provide parameters for the dynamic programming.

B. DYNAMIC PROGRAMMING

The dynamic programming is suitable for linear and nonlinear systems, and adopted to obtain the optimal motor braking torques and wheel cylinder pressures for the vehicle control.

The dynamic programming must determine parameters such as decision variables, state variables, and index functions. The required braking torques of the front and rear motors and the required cylinder pressures of the front and rear wheels are selected as the decision variables, that is, the decision variables are $[T_{m1}, T_{m2}, p_{w1}, p_{w2}]^T$. The decision variables must respect the legal requirements. The braking force distribution coefficient is closely related to the decision variable. The relationship among the braking force distribution coefficient, front and rear axle braking torques, and total braking torque is

$$\begin{cases} T_f = p_{w1} \pi D_f^2 R_f K_f / 2 + T_{m1} i_1 / \eta_1 \\ T_r = p_{w2} \pi D_r^2 R_r K_r / 2 + T_{m2} i_2 / \eta_2 \\ T_t = T_f + T_r \\ \beta = T_f / T_t \end{cases} \quad (20)$$

where β is the braking force distribution coefficient. T_f and T_r are the braking torques at the front and rear wheel ends, respectively, and T_t is the total braking torque provided by the wheel ends.

The braking torques of the front and rear axles are constrained by the maximum braking torque on the ground.

$$\begin{cases} T_f \leq \mu_0 mg(b + zh_g) R_t / L \\ T_r \leq \mu_0 mg(c - zh_g) R_t / L \end{cases} \quad (21)$$

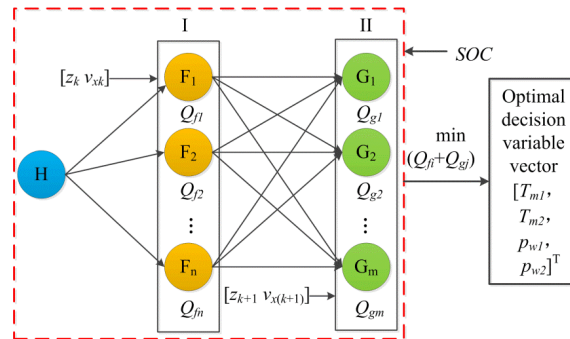


FIGURE 6. Schematic diagram of the dynamic programming optimization process.

where μ_0 is the road adhesion coefficient. The right end of the equation represents the maximum braking torques (wheel ends) that the ground can provide.

In the process of vehicle braking, the braking force distribution coefficient must respect the requirements of the ECE regulations.

$$\beta \leq (z + 0.07)(b + zh_g) / (0.85zL), \quad z \in [0.1, 0.61] \quad (22)$$

$$\beta \geq 1 - (z + 0.05)(c - zh_g) / (zL), \quad z \in [0.3, 0.45] \quad (23)$$

$$\beta \geq (b + zh_g) / L, \quad z \in [0.15, 0.8] \quad (24)$$

Equation (22) is the upper limit required by the ECE when the braking intensity is between 0.1 and 0.6, to prevent the front axle from distributing an excessive braking force. Equation (23) is the lower limit required by the ECE when the braking intensity is between 0.3 and 0.45 to prevent the rear axle from distributing an excessive braking force. Equation (24) is the middle limit required by the ECE when the braking intensity is between 0.15 and 0.8.

In the process of vehicle braking, the motor torques are also constrained by the vehicle transmission system itself. If the braking torques are overly large, the vehicle produces an abnormal noise. The vehicle transmission system constraints (referred to as the vehicle constraints) are

$$\begin{cases} |T_{m1}| i_1 \eta_1 / R_t \leq \gamma_1 \delta mg \\ |T_{m2}| i_2 \eta_2 / R_t \leq \gamma_2 \delta mg \end{cases} \quad (25)$$

where γ_1 and γ_2 are the maximum proportional coefficients of the vehicle front and rear axle transmission systems that do not emit abnormal noise, respectively.

The braking torque of the motor is also constrained by the motor itself.

$$\begin{cases} |T_{m1}| \leq |T_{mf \max}| \\ |T_{m2}| \leq |T_{mr \max}| \end{cases} \quad (26)$$

where $T_{mf \max}$ and $T_{mr \max}$ are the maximum braking torques of the front and rear motors, respectively.

The selection of the index function in the dynamic programming is extremely important for its optimization. The energy recovery by the battery is selected as the index function, which can be obtained by combining Equations (5)

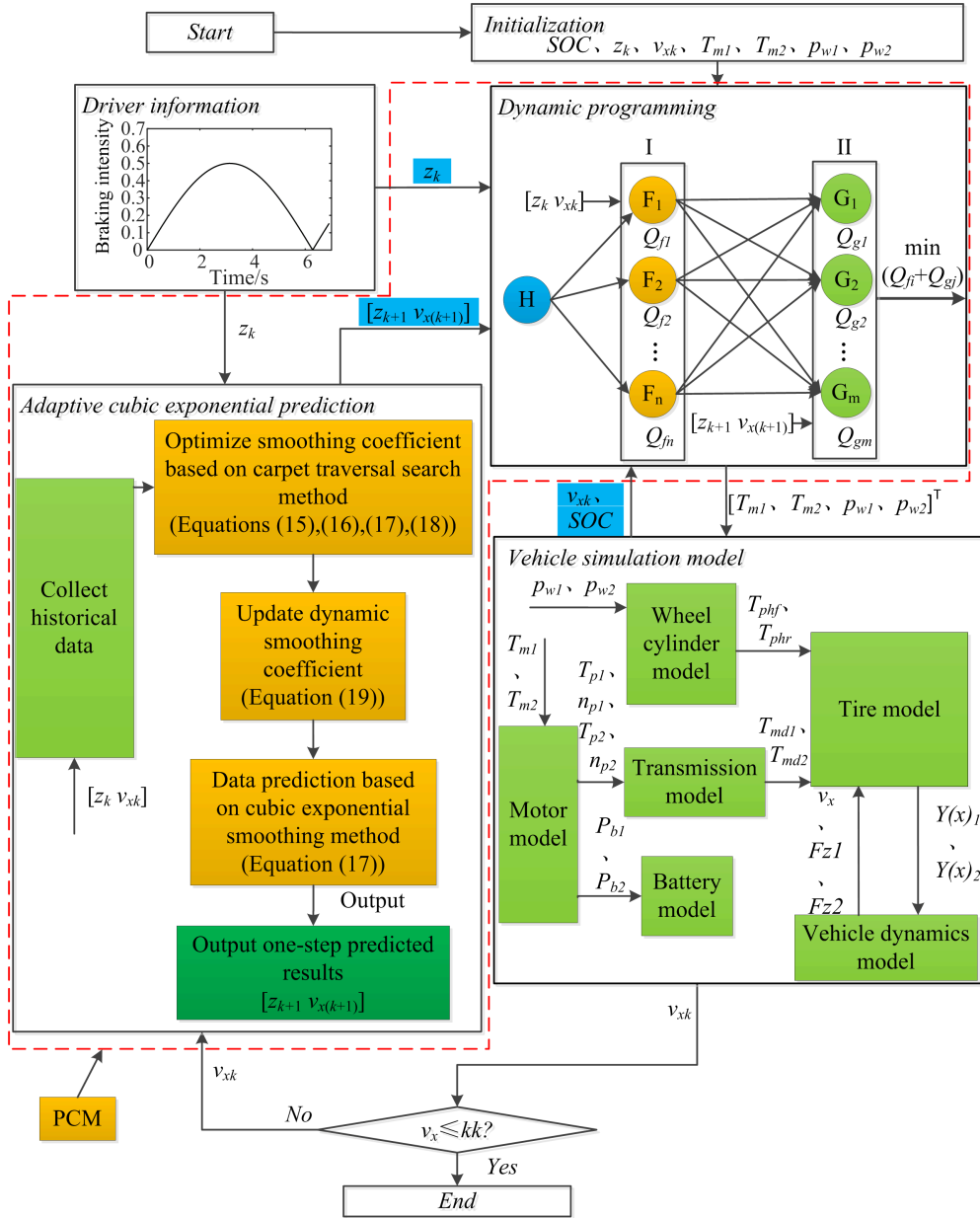


FIGURE 7. Framework of PCM.

and (8):

$$Q = - \int (|T_{p1}n_{p1}\eta_{m1}/9550 + T_{p2}n_{p2}\eta_{m2}/9550| - I^2r) dt \quad (27)$$

Front and rear motor efficiencies η_{m1} and η_{m2} , respectively, are related to the speeds (n_{p1} and n_{p2}) and torques (T_{p1} and T_{p2}) of the motors, which can be obtained by consulting the table (motor efficiency maps). The current I can be obtained by Equation (8).

The selection of the state variables should be combined with the control object. This study considers the dynamic characteristics of the front and rear motors and the braking

wheel cylinders. The means of the interferogram call are used for the simulation test. Therefore, the motor braking torques and wheel cylinder pressures are used as state variables, that is, the state variables are $[T_{m1}, T_{m2}, p_{w1}, p_{w2}]^T$. Because the state variables are consistent with the decision variables, the decision process of the dynamic programming is the state transition process.

The schematic diagram of the dynamic programming optimization process is shown in Figure 6. This study adopts two-stage dynamic programming, as one-step forecast of adaptive cubic exponential prediction is the most accurate. The $[z_k, v_{xk}]$ and $[z_{k+1}, v_x(k+1)]$ act on the stages I and II, respectively. The SOC is considered approximately constant

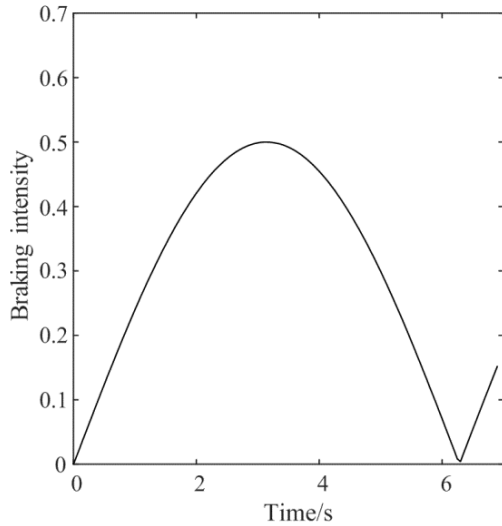


FIGURE 8. Gradual braking conditions.

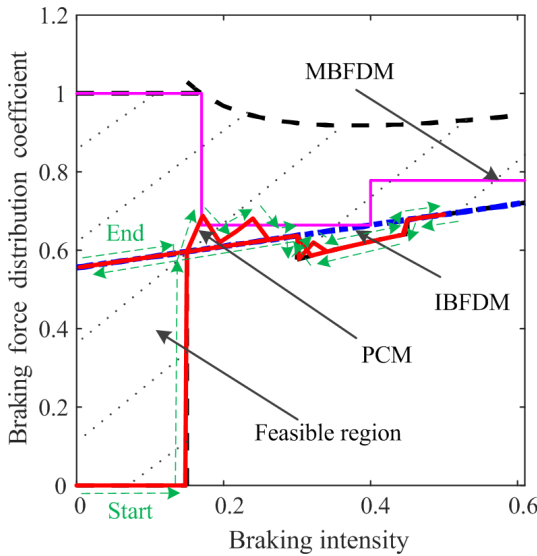


FIGURE 9. Braking force distribution coefficients.

throughout the process. Q_{fn} and Q_{gm} represent the index function values of states F_n and G_m , respectively, which are obtained by the predictive vehicle model. When $\min(Q_{fi} + Q_{gj})$ ($i = 1, 2, \dots, n; j = 1, 2, \dots, m$), the stage I optimal decision variable vector is obtained $[T_{m1}, T_{m2}, p_{w1}, p_{w2}]^T$.

C. PCM FRAMEWORK

The PCM integrates adaptive cubic exponential prediction and dynamic programming. In this study, the operating condition information is set to the gradient braking intensity, which is obtained from the driver’s model and simulated via a sine function [35].

$$z = abs(\sin(t/2))/2 \tag{28}$$

A framework of the PCM is displayed in Figure 7. The PCM is indicated by the red dotted line. First, the model is

initialized with the battery SOC, vehicle velocity v_{xk} , braking intensity z_k , front and rear wheel required cylinder pressures p_{w1} and p_{w2} , respectively, front and rear motor required torques T_{m1} and T_{m2} , respectively.

The dynamic programming calls the predictive vehicle model to optimize T_{m1}, T_{m2}, p_{w1} , and p_{w2} under the constraint conditions (Equations (21), (22), (23), (24), (25), (26)) to maximize the battery energy recovery.

Then, the vehicle simulation model outputs v_{xk} . Next, v_{xk} is evaluated: if it is lower than kk (kk is a constant), the simulation terminates; otherwise, the v_{xk} is output to the adaptive cubic exponential prediction. This prediction relies on v_{xk} and z_k to obtain the predicted vectors $[z_{k+1} \ v_{x(k+1)}]$, and then sends them to the dynamic programming for the next optimal control. This is repeated until v_{xk} becomes lower than kk . It is important to note that the adaptive cubic exponential prediction must collect information (several sampling points) before making a prediction. Only the stage I optimization is performed in dynamic programming at the first few sampling points.

IV. SIMULATION VERIFICATION AND DISCUSSION

The effectiveness of vehicle control can be verified via simulation. This study verifies the PCM using a simulation test. When the vehicle velocity is low, energy recovery is not performed to protect the motors. The main technical parameters of the vehicle are listed in Table 1.

TABLE 1. Main technical parameters of the vehicle.

Project	Parameter	Numerical value
Vehicle	Curb mass m / kg	1880
	Height of gravity center h_g / m	0.8
	Distance from center of gravity to front axle c / m	1.29
	Distance from center of gravity to rear axle b / m	1.61
Front motor	Wheelbase L / m	2.90
	Rated power / kw	45
Rear motor	Peak torque / Nm	242
	Rated power / kw	50
Battery	Peak torque / Nm	283
	Capacity / Ah	234
Main reducer I	Nominal voltage / v	320
	Transmission ratio i_1	9.01
Main reducer II	Transmission ratio i_2	9.01
	Wheel cylinder diameter D_f / mm	49
Front wheel cylinder	Braking factor K_f	0.8
	Braking action radius R_f / mm	120
Rear wheel cylinder	Wheel cylinder diameter D_r / mm	21
	Braking factor K_r	0.8
	Braking action radius R_r / mm	120

The PCM is compared with the multi-stage braking force distribution method (MBFDM), commonly used in engineering, and the ideal braking force distribution method (IBFDM). The initial vehicle velocity was set to 75 km/h, the battery SOC was set to 70%, and a road with acceptable conditions was used as the simulated road; the road adhesion coefficient was 0.82. The gradual braking conditions [35] change as indicated in Figure 8.

The braking force distribution coefficients of the MBFDM, IBFDM, and PCM are displayed in Figure 9. The constraints for the above methods were the same. In Figure 9, the shaded area is the feasible region of the braking force distribution coefficient prescribed by the ECE regulations. The braking force distribution coefficients of the three methods are within the feasible range. The blue dotted, pink, and red lines represent the curve of the braking force distribution coefficient used by the IBFDM, MBFDM, and PCM, respectively. Among these, the braking force distribution coefficients of the IBFDM and MBFDM are only related to the braking intensity, whereas that of the PCM is zero at the initial stage of braking, and then changes in the direction of the arrow, indicating that the braking force distribution coefficient is related to the braking intensity and also to the vehicle velocity.

The changes in the front and rear motor braking torques under the three control methods are indicated in Figures 10(a) and (b), respectively, including a comparison of

the required and actual braking torques. PCMD, MBFDMD, and IBFDMD are the required braking torques and PCDA, MBFDMA, and IBFDMA are the actual braking torques of the PCM, MBFDM, and IBFDM, respectively. The braking torque changes of the three control methods under the same braking intensity are not exactly the same, and the maximum braking torque attains the vehicle constraint (refer to the limit Equation (25) for the transmission system not to emit an abnormal noise). The enlarged sections indicate that the actual braking torques of the front and rear motors are not exactly the same as the required braking torques. However, they are consistent with the required braking torques at the end of the control duration. The braking torque is higher than zero owing to overshoot during the torque change of the motor.

The changes in the front and rear wheel cylinder pressures under the three control methods are presented in Figures 11(a) and (b), respectively, including also a

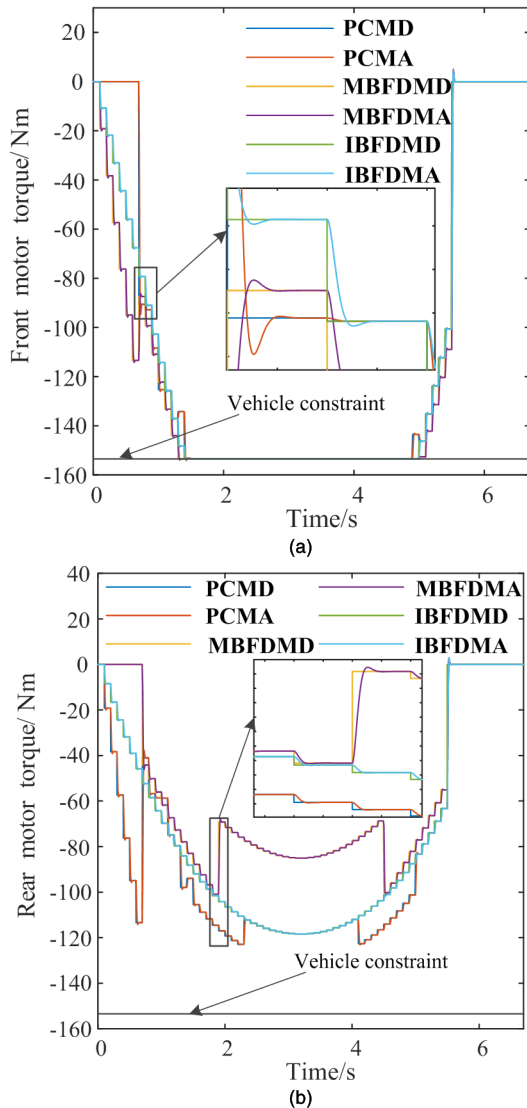


FIGURE 10. Braking torque changes of motors.

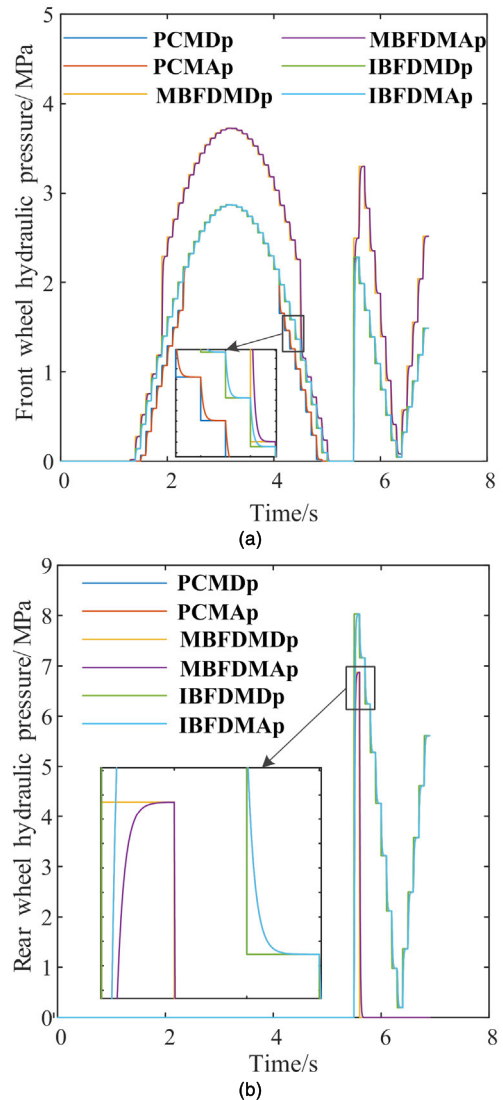


FIGURE 11. Wheel cylinder pressure changes of front and rear wheels.

comparison of the required and actual wheel cylinder pressures. PCMDp, MBFDMDp, and IBFDMDp are the wheel required cylinder pressures and PCMAp, MBFDMAp and IBFDMAp are the actual wheel cylinder pressures of the PCM, MBFDM, and IBFDM, respectively. The wheel cylinder pressure changes of the three control methods under the same braking intensity are not exactly the same. From the enlarged section in Figure 11, we can observe that the actual and required wheel cylinder pressures are not completely consistent. However, at the end of the control duration, they are consistent with each other.

The changes in the battery SOC of the three control methods are displayed in Figure 12. The SOC started to increase from 70%. The final SOC of the PCM, MBFDM, and IBFDM were 70.104%, 70.095%, and 70.102%, respectively. The SOC under the PCM increased the most.

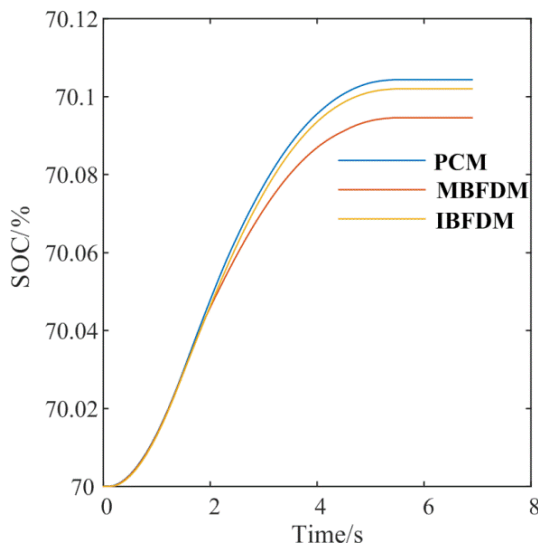


FIGURE 12. Battery SOC changes.

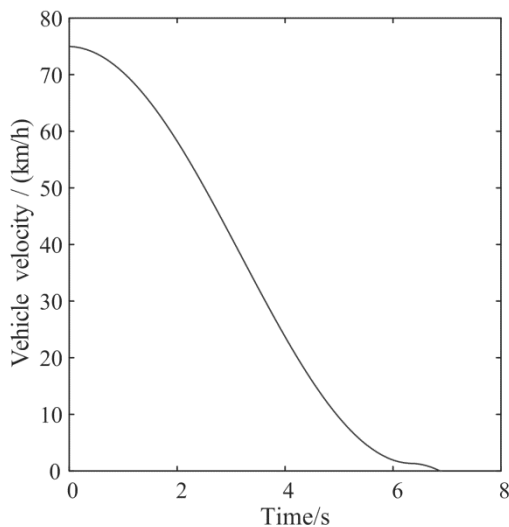


FIGURE 13. Vehicle velocity changes.

The changes in vehicle velocity are displayed in Figure 13. Combining Figure 10 we can see that when the vehicle velocity is low, the motors are off.

The vehicle energy flow is displayed in Figure 14. The braking energy is converted into four parts of energy, which are wind resistance loss, rolling resistance loss, ramp resistance loss, and recoverable energy. Recoverable energy (red dotted part) is stored from the wheel through the reducers to the motors and even to the battery, but the battery is the key to improving energy conversion efficiency. During the energy conversion process, energy loss occurs at the wheels, main reducers I and II, front and rear motors, and battery.

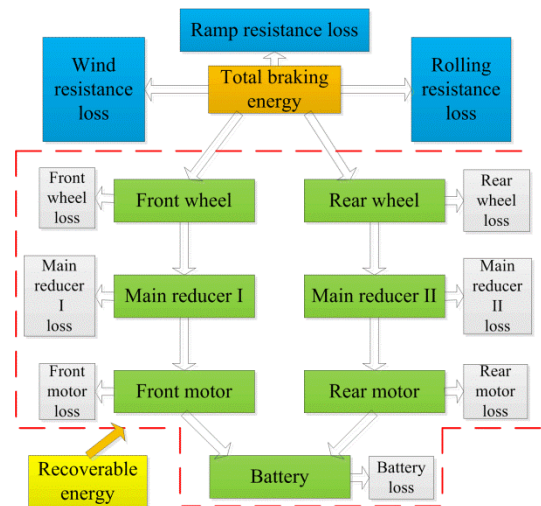


FIGURE 14. Vehicle energy flow.

The effective energy of the components, shown in Figure 15, refers to the energy flowing out of the component or the energy stored. It can be seen from Figure 15 that under different control methods, the energy stored by the battery

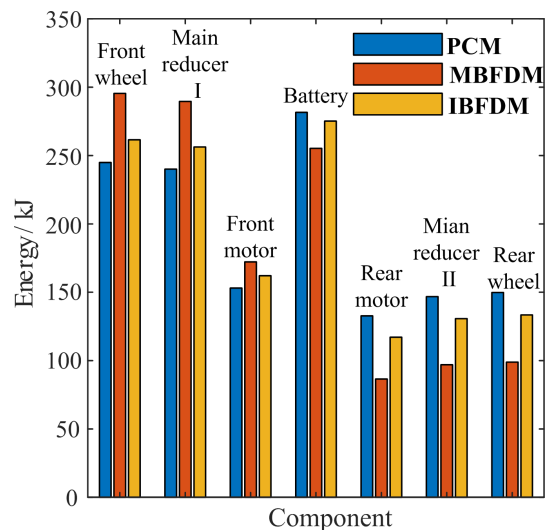


FIGURE 15. Effective energy of component.

is different. The recovered energies via PCM, IBFDM, and MBFDM during the entire braking process were 281.63 kJ, 275.25 kJ, and 255.25 kJ, respectively. When compared with the IBFDM and MBFDM, PCM increased energy recovery efficiency by 1.55% and 6.40%, respectively.

The changes in the front and rear motor braking efficiencies under the three control methods are indicated in Figures 16(a) and (b), respectively. Among the three control methods, the front and rear motor efficiency of PCM is not always the most efficient. At the initial stage of braking, the front motor under PCM and rear motor under MBFDM are not working (when efficiency is equal to zero, it means that the motor is off). The enlarged sections show that the motor efficiencies are different under different control methods.

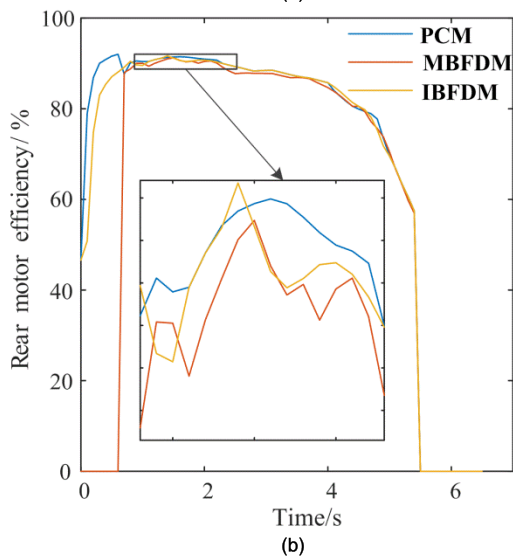
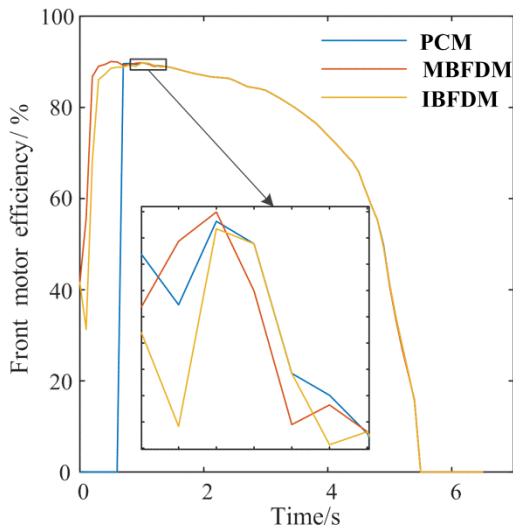


FIGURE 16. Changes in motor efficiency.

The battery efficiency change, shown in Figure 17, indicates that, among the three control methods, battery

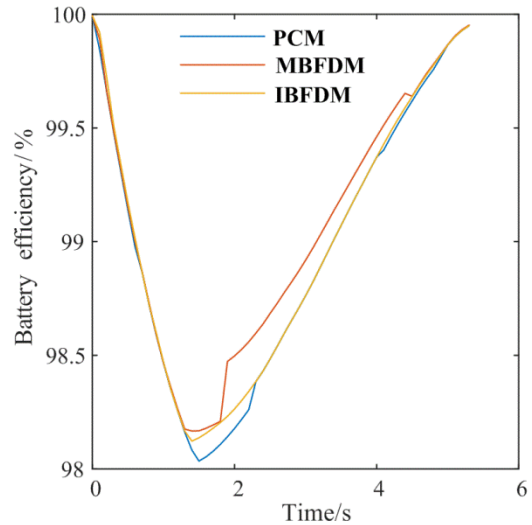


FIGURE 17. Changes in battery efficiency.

efficiency of PCM is the smallest, and the MBFDM, which recovers the least energy, has the highest battery efficiency for a long time. Combining Figures 16 and 17, we can see that it is difficult to achieve maximum energy conversion efficiency for dual-motor-driven vehicles simply by aiming for maximum efficiency of a single component.

Figure 18 shows the changes in the total efficiency of the vehicle (which includes the efficiency of the motors, battery, and transmission system) under the three control methods. The total efficiency of the vehicle under PCM is the largest, whereas that under MBFDM is the smallest for a long-term in the entire braking process. This indicates the superiority of PCM.

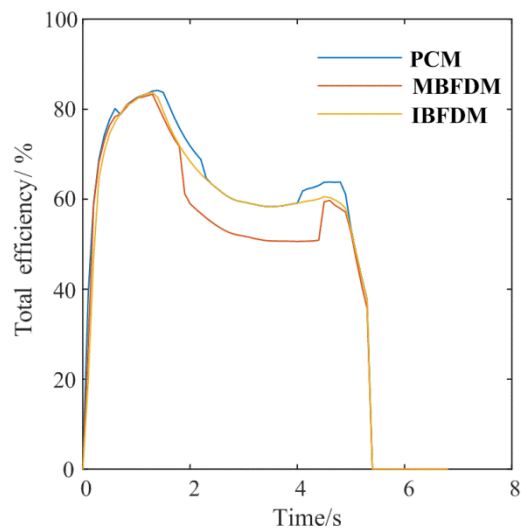


FIGURE 18. Changes in total efficiency.

In summary, simulations of the three control methods were conducted under a gradual braking condition, and the changes in braking force distribution coefficients are displayed

in Figure 9. The changes in the front and rear motor torques, presented in Figures 10(a) and (b), respectively, indicate that the actual braking torques of the front and rear motors are not exactly the same as the required braking torques. The pressure changes of the front and rear wheel cylinders under the three methods, presented in Figures 11(a) and (b), respectively, indicate that there is no hydraulic pressure on the rear wheels to participate at the early stage of braking. As seen in Figure 12, the SOC under the PCM increased the most. The changes in vehicle velocity are displayed in Figure 13. The vehicle energy flow and effective energy of the components, displayed in Figures 14 and 15, respectively, indicate that the PCM provides a higher energy recovery. The changes in the front and rear motor braking efficiencies, displayed in Figures 16(a) and (b), respectively, indicate that the front and rear motor efficiencies of PCM are not always the best. The changes in battery and total vehicle efficiencies, shown in Figures 17 and 18, respectively, indicate that the total efficiency of the vehicle under PCM is the largest in the entire braking process.

V. CONCLUSION

Energy recovery is a key technology to improve the driving range of pure electric vehicles. To improve the energy recovery efficiency during vehicle braking, the vehicle longitudinal control method under regular braking conditions is studied, and a PCM based on adaptive cubic exponential prediction and dynamic programming is proposed. The predictive optimization framework of PCM is presented for the first time. The adaptive cubic exponential prediction uses the historical data of the vehicle, predicts future key parameters such as vehicle velocity and braking intensity, and provides parameter support for the dynamic programming. The dynamic programming optimizes the front and rear motor braking torques, and front and rear wheel cylinder pressures to provide control parameters for the vehicle. To verify the superiority of the proposed method, simulations were performed under gradual braking conditions. The results indicated that the energy recovery of the proposed PCM increased by 1.55% and 6.40%, compared with the IBFDM and MBFDM, respectively. Moreover, this study provides new ideas for regenerative braking energy recovery.

REFERENCES

- [1] N. O. Bonsu, "Towards a circular and low-carbon economy: Insights from the transitioning to electric vehicles and net zero economy," *J. Cleaner Prod.*, vol. 256, May 2020, Art. no. 120659.
- [2] K. Kim and Y. Kim, "International comparison of industrial CO₂ emission trends and the energy efficiency paradox utilizing production-based decomposition," *Energy Econ.*, vol. 34, no. 5, pp. 1724–1741, Sep. 2012.
- [3] J. Qi, L. Liu, Z. Shen, B. Xu, K.-S. Leung, and Y. Sun, "Low-carbon community adaptive energy management optimization toward smart services," *IEEE Trans. Ind. Informat.*, vol. 16, no. 5, pp. 3587–3596, May 2020.
- [4] D. Bresser, K. Hosoi, D. Howell, H. Li, H. Zeisel, K. Amine, S. Passerini, "Perspectives of automotive battery R&D in China, Germany, Japan, and the USA," *J. Power Sources*, vol. 382, pp. 176–178, Apr. 2018.
- [5] X. Jin, Z. Yu, G. Yin, and J. Wang, "Improving vehicle handling stability based on combined AFS and DYC system via robust Takagi-Sugeno fuzzy control," *IEEE Trans. Intell. Transp. Syst.*, vol. 19, no. 8, pp. 2696–2707, Aug. 2018.
- [6] X. Jin, G. Yin, X. Zeng, and J. Chen, "Robust gain-scheduled output feedback yaw stability control for in-wheel-motor-driven electric vehicles with external yaw-moment," *J. Franklin Inst.*, vol. 355, no. 18, pp. 9271–9297, Dec. 2018.
- [7] X. Jin, J. Yang, Y. Li, B. Zhu, J. Wang, and G. Yin, "Online estimation of inertial parameter for lightweight electric vehicle using dual unscented Kalman filter approach," *IET Intell. Transp. Syst.*, vol. 14, no. 5, pp. 412–422, 2020.
- [8] J. Zhang, C. Lv, J. Gou, and D. Kong, "Cooperative control of regenerative braking and hydraulic braking of an electrified passenger car," *Proc. Inst. Mech. Eng., Part D, J. Automobile Eng.*, vol. 226, no. 10, pp. 1289–1302, 2012.
- [9] X. Dong, B. Zhang, B. Wang, and Z. Wang, "Urban households' purchase intentions for pure electric vehicles under subsidy contexts in China: Do cost factors matter?" *Transp. Res. A, Policy Pract.*, vol. 135, pp. 183–197, May 2020.
- [10] Z. Li, A. Khajepour, and J. Song, "A comprehensive review of the key technologies for pure electric vehicles," *Energy*, vol. 182, pp. 824–839, Sep. 2019.
- [11] Z. Zhang, Y. Dong, and Y. Han, "Dynamic and control of electric vehicle in regenerative braking for driving safety and energy conservation," *J. Vib. Eng. Technol.*, vol. 8, no. 1, pp. 179–197, 2020.
- [12] M. Passalacqua, M. Carpita, S. Gavin, M. Marchesoni, M. Repetto, L. Vaccaro, and S. Wasterlain, "Supercapacitor storage sizing analysis for a series hybrid vehicle," *Energies*, vol. 12, no. 9, p. 1759, May 2019.
- [13] W. Li, H. Du, and W. Li, "Four-wheel electric braking system configuration with new braking torque distribution strategy for improving energy recovery efficiency," *IEEE Trans. Intell. Transp. Syst.*, vol. 21, no. 1, pp. 87–103, Jan. 2020.
- [14] C. Zheng, W. Li, and Q. Liang, "An energy management strategy of hybrid energy storage systems for electric vehicle applications," *IEEE Trans. Sustain. Energy*, vol. 9, no. 4, pp. 1880–1888, Oct. 2018.
- [15] U. Diego-Ayala, P. Martinez-Gonzalez, N. McGlashan, and K. R. Pullen, "The mechanical hybrid vehicle: An investigation of a flywheel-based vehicular regenerative energy capture system," *Proc. Inst. Mech. Eng., D, J. Automobile Eng.*, vol. 222, no. 11, pp. 2087–2101, 2008.
- [16] Q. S. Feng and H. Li, "Design of electric vehicle energy regenerative braking system based on super capacitor," *Appl. Mech. Mater.*, vol. 157, pp. 53–149, Feb. 2012.
- [17] A. P. Budijono, I. N. Sutantra, and A. S. Pramono, "Ratchet flywheel regenerative system to enhance energy captured for electric vehicle," in *Proc. AIP Conf.*, 2019, vol. 2187, no. 1, Art. no. 020040.
- [18] R. T. Meyer, R. A. DeCarlo, and S. Pekarek, "Hybrid model predictive power management of a battery-supercapacitor electric vehicle," *Asian J. Control*, vol. 18, no. 1, pp. 150–165, 2016.
- [19] A. González-Gil, R. Palacin, and P. Batty, "Sustainable urban rail systems: Strategies and technologies for optimal management of regenerative braking energy," *Energy Convers. Manage.*, vol. 75, pp. 374–388, Nov. 2013.
- [20] H. Liu, Y. Lei, Y. Fu, and X. Li, "Multi-objective optimization study of regenerative braking control strategy for range-extended electric vehicle," *Appl. Sci.*, vol. 10, no. 5, p. 1789, Mar. 2020.
- [21] H. Liu, Y. Lei, Y. Fu, and X. Li, "An optimal slip ratio-based revised regenerative braking control strategy of range-extended electric vehicle," *Energies*, vol. 13, no. 6, p. 1526, Mar. 2020.
- [22] Y. Yang, Q. He, Y. Chen, and C. Fu, "Efficiency optimization and control strategy of regenerative braking system with dual motor," *Energies*, vol. 13, no. 3, p. 711, Feb. 2020.
- [23] S. Li, B. Yu, and X. Feng, "Research on braking energy recovery strategy of electric vehicle based on ECE regulation and I curve," *Sci. Prog.*, vol. 103, no. 1, Jan. 2020, Art. no. 003685041987776.
- [24] L. Liu, F. Ji, S. Yang, and B. Xu, "Control strategy for electro-mechanical braking based on curves of ECE regulations and ideal braking force," *J. Beijing Univ. Aeronaut. Astronaut.*, vol. 39, no. 1, pp. 138–142, 2013.
- [25] F. Ji, Y. Pan, Y. Zhou, F. Du, Q. Zhang, and G. Li, "Energy recovery based on pedal situation for regenerative braking system of electric vehicle," *Vehicle Syst. Dyn.*, vol. 58, no. 1, pp. 144–173, 2020.
- [26] C. S. N. Kumar and S. C. Subramanian, "Cooperative control of regenerative braking and friction braking for a hybrid electric vehicle," *Proc. Inst. Mech. Eng., D, J. Automobile Eng.*, vol. 230, no. 1, pp. 103–116, 2016.
- [27] J. Ko, S. Ko, H. Son, B. Yoo, J. Cheon, and H. Kim, "Development of brake system and regenerative braking cooperative control algorithm for automatic-transmission-based hybrid electric vehicles," *IEEE Trans. Veh. Technol.*, vol. 64, no. 2, pp. 431–440, Feb. 2015.

- [28] Z. Liu, S. Lu, and R. Du, "A genetic-fuzzy control method for regenerative braking in electric vehicle," *Int. J. Comput. Sci. Math.*, vol. 11, no. 3, pp. 263–277, 2020.
- [29] X. Pei, H. Pan, Z. Chen, X. Guo, and B. Yang, "Coordinated control strategy of electro-hydraulic braking for energy regeneration," *Control Eng. Pract.*, vol. 96, Mar. 2020, Art. no. 104324.
- [30] H. He, C. Wang, H. Jia, and X. Cui, "An intelligent braking system composed single-pedal and multi-objective optimization neural network braking control strategies for electric vehicle," *Appl. Energy*, vol. 259, Feb. 2020, Art. no. 114172.
- [31] S. Cheng, L. Li, X. Chen, S.-N. Fang, X.-Y. Wang, X.-H. Wu, and W.-B. Li, "Longitudinal autonomous driving based on game theory for intelligent hybrid electric vehicles with connectivity," *Appl. Energy*, vol. 268, Jun. 2020, Art. no. 115030.
- [32] Y. G. Luo, P. Li, D. Jin, and K. Li, "A study on regenerative braking strategy based on optimal control theory," *Automot. Eng.*, vol. 28, no. 4, pp. 356–360, 2006.
- [33] A. Ružinskas and H. Sivilevičius, "Magic formula tyre model Application for a tyre-ice interaction," in *Proc. 10th Int. Sci. Conf.*, vol. 187, May 2017, pp. 335–341, doi: [10.1016/j.proeng.2017.04.383](https://doi.org/10.1016/j.proeng.2017.04.383).
- [34] G. Q. Wang, S. Wang, H. Y. Liu, Y. D. Xue, and Z. Ping, "Self-adaptive and dynamic cubic ES method for wind speed forecasting," *Power Syst. Protection Control*, vol. 42, no. 15, pp. 117–122, 2014.
- [35] Z. Wang, "Research on control strategy and test technology of electromechanical combined braking for electric drive tracked vehicle," Ph.D. dissertation, Zhejiang Univ., Hangzhou, China, 2019.



JUNJIANG ZHANG was born in Zhoukou, Henan. He received the B.S. degree in mechanical engineering from the Luoyang Institute of Science and Technology, in 2014, and the M.S. degree from the Vehicle and Transportation Engineering Institute, Henan University of Science and Technology, Luoyang, China, in 2017. He is currently pursuing the Ph.D. degree in vehicle engineering with Chongqing University. His main research interest includes electric vehicles control.



vehicle power transmission systems and electronic control.

YANG YANG (Member, IEEE) received the B.S. and M.S. degrees in mechanical engineering from Chongqing Jianzhu University, Chongqing, China, in 1982 and 1986, respectively, and the Ph.D. degree in mechanical engineering from Chongqing University, Chongqing, in 2008. He is currently a Professor with the Automotive Engineering Department, Chongqing University. He has authored or coauthored more than 60 academic articles. His current research interests include



DATONG QIN (Member, IEEE) was born in Chongqing, China, in 1956. He received the B.S., M.S., and Ph.D. degrees in mechanical engineering from Chongqing University, in 1982, 1984, and 1993, respectively. From 1989 to 1991, he was a Visiting Scholar with the Department of Precision Engineering, Tohoku University, Japan. From 1995 to 1997, he was the Deputy Director of SKLMT, China. He is currently a Professor with the School of Automotive Engineering, Chongqing University. He was awarded as the Changjiang Chair Professor, in 2005. His research interests include gear transmission systems, and dynamic modeling and control of driveline systems of vehicle.



CHUNYUN FU received the B.S. degree from Chongqing University, Chongqing, China, in 2010, and the Ph.D. degree from RMIT University, Melbourne, VIC, Australia, in 2015. He is currently a Lecturer with the Automotive Engineering Department, Chongqing University. He has published over 20 articles in reputable journals and conference proceedings. His main research interests include autonomous vehicles and electric vehicles.



ZHIPENG CONG received the B.S. degree in vehicle engineering from Chongqing University, Chongqing, China, in 2018, where he is currently pursuing the M.S. degree. His research interests include vehicle power transmission systems and electronic control.

...